Ultrasonics 116 (2021) 106504

Contents lists available at ScienceDirect

Ultrasonics

journal homepage: www.elsevier.com/locate/ultras

Experimental and simulation study of harmonic components generated by plane and focused waves

Francesco Guidi [a,*], Libertario Demi [b], Piero Tortoli [a]

[a] Department of Information Engineering, University of Florence, Florence, Italy
[b] Department of Information Engineering and Computer Science, University of Trento, Trento, Italy

ARTICLE INFO

Keywords:
Nonlinear propagation
Plane waves
Focused waves
Harmonic imaging
ULA-OP

ABSTRACT

Although there is increasing interest in the use of plane waves (PW) in high-frame-rate imaging, not much experimental data is available about their behavior in terms of nonlinear propagation. This paper presents a detailed study of fundamental and harmonic components of the ultrasound beam associated to PW transmission from a linear array. Simulations and hydrophone measurements of PW propagation in water were performed and compared to the results obtained for focused waves (FWs) at various levels of peak negative pressure (PNP). Experimental results confirm that, at comparable PNP, the amplitudes of the harmonics reached by PWs are always higher, over extended regions, than those achieved with FW. For example, at MI = 0.2 the PW second harmonic turns out to be 9 dB higher at 25 mm depth (i.e. in the focal region), and 20 dB higher at 40 mm depth. Simulations additionally show that when ultrasound waves propagate through blood or muscle, the situation is in general reversed but, at low MI, the second harmonic amplitude can still be higher in PW than in FW. Furthermore, it is shown that increasing the array aperture size yields higher harmonic growth in PW compared to FW.

1. Introduction

Plane Wave (PW) transmission allows reaching high frame rates in ultrasound imaging by minimizing the number of transmission events necessary to form an image [1]. If the elements are fired at the same instant, the transmitted ultrasound beam generally shows an almost constant beamwidth and a peak pressure field amplitude which varies gently over depth [2]. Differently, Focused Wave (FW) transmission has the effect of locally maximizing the peak pressure and minimizing the beamwidth around the focal point. Focusing also implies that both the peak pressure amplitude and the beam-width will vary significantly over depth [2].

Because of these differences, when the same transducer array is used, and in case the peak pressure generated at the source is for both identical, FW would produce a significantly higher pressure compared to PW. For this reason, FW is the method of choice for Tissue Harmonic Imaging (THI) and Super Harmonic Imaging (SHI). In fact, with these techniques, ultrasound images are formed exploiting only the harmonic components associated with the pressure field, and high peak pressure is essential for the development of strong harmonic components. Harmonic growth is a nonlinear process [3] and is due to the pressure dependency of the speed of sound causing a cumulative deformation of the originally transmitted waveforms. The higher the generated peak pressure, the stronger the deformation experienced by the wave and the higher the amplitude of the harmonics. Compared to standard ultrasound imaging, which exploits only the fundamental component of the generated pressure wavefield, THI and SHI improve the spatial resolution, reduce the effects of side and grating lobes, and diminish clutter effects [4–6].

Indeed, the amplitude of harmonic components generated by tissue nonlinearities does not depend solely on the generated peak pressure amplitude, but it is also strongly influenced by the spatial distribution of the pressure field amplitude. The fundamental pressure wavefield (i.e. the field content centered around the transmitted center frequency) can be seen as a distributed source of nonlinearity [7]. Consequently, the combined effect of a great number of weak sources, such as with PW, could potentially result in the generation of stronger harmonic components as compared with the effect of few strong sources, as with FW. It is therefore interesting to study the harmonic component amplitudes generated by PW and FW when applied at equal MI.

This topic has been recently approached in different ways. Analytical models for plane progressive sound waves propagation in non-

* Corresponding author.

https://doi.org/10.1016/j.ultras.2021.106504
Received 1 December 2020; Received in revised form 21 May 2021; Accepted 17 June 2021
Available online 22 June 2021
0041-624X/

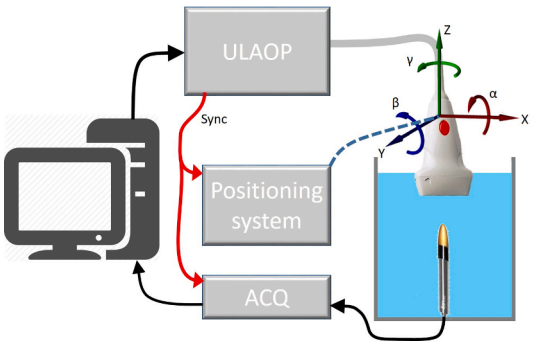

Fig. 1. Setup block diagram.

dissipative [8] fluids as well as for focused beams [9,10] have been introduced. A numerical study based on a KZK model was performed by Lai et al. In [11], the authors studied the second harmonic amplitude generated by the transmission of PW from diagnostic arrays. Since this work was focused on the applicability of PW to THI, only the highest possible mechanical index (MI = 1.9) was investigated. In these conditions, the second harmonic generated in tissue with PW, when compared with FW, was found to be generally lower (2–16 dB lower). On the other hand, Guidi et al [12] reported on experimental measurements performed in water, at low MIs (0.1 and 0.2), which showed that the second and third harmonic amplitudes are generally higher for PW compared to FW.

The objective of this work was to conduct a comparative analysis of nonlinear fields generated by PW and FW for equal MI over a large range of values. To this end, experiments, as well as a numerical study based on freeware simulation tools, were performed. Experiments included hydrophone measurements in water, with varying MI (0.05–0.7) and center-frequency (3–7 MHz). The impact of absorption through different media and of array aperture was numerically investigated at 3 and 4 MHz for a range of MI values from 0.05 to 1.2.

The paper is organized as follows. Sections 2 and 3 illustrate the setups and corresponding results related to the experimental and numerical study, respectively. Section 4 contains the discussion on the reported findings. The conclusions are drawn in Section 5.

2. Experimental study

2.1. Experimental set-up

The experimental work was based on the ULA-OP research scanner [13], which can be programmed to transmit either focused and plane waves. ULA-OP was coupled to the LA332 (Esaote, Florence, Italy), a 144-element linear array with 245 μm pitch, 30 μm kerf, 4.6 MHz center frequency, and 100% (−6 dB) bandwidth. Whichever transmission modality was activated, the silicon lens covering the elements established an elevational focus at about 23 mm.

The 64 central elements of the probe were excited by sinusoidal bursts with central frequency in the range of 3–7 MHz. Each burst was Hanning weighted and the length was adjusted to ensure a −6 dB bandwidth of 1 MHz at all transmission (TX) frequencies. The TX signals were beamformed to produce waves with programmable PNP and focal depth. The probe was moved through a water volume of 20 × 3 × 40 mm by a 6-axis positioning system (see Fig. 1) and the ultrasound beam obtained in each experimental condition was measured using the HGL008 hydrophone (Onda Corporation, Sunnyvale, CA, USA). The hydrophone's electrode, having an 85 μm aperture, was connected to a low noise amplifier (Onda, mod. AH-2010) followed by a 12-bit Analog-to-Digital Converter working at 125 MSPS. Both the probe displacement and the acquisition of ultrasound radiofrequency (RF) signals by the hydrophone were triggered by the TX pulses. The full volumetric beam plots around the beam axis were thus obtained over the 10–50 mm depth range with 0.3 mm spatial resolution.

In each experiment, the probe was carefully oriented acting on the alpha, beta, gamma angles (see Fig. 1), to align the array surface with the XZ plane of the positioning system, and the acoustic axis with the hydrophone axis. The data acquired by the hydrophone were converted to Pascal through the hydrophone calibration curve. The data were then processed to extract the PNP values of the total field and, after 4° order bandpass filtering (3-dB bandwidth: 3 MHz), the peak values for each of the harmonic components.

Most acquisitions were performed in a low distortion regime (MI < 0.2), to permit, by adjusting the TX signal amplitude, an empirical PNP equalization. As specified below, in some experiments, the TX signal amplitudes were increased to produce MIs over the range 0,07–0,7.

B. Experimental results

Fig. 2 allows comparing the XZ beam-plots obtained when waves focused at 25 mm (left) or a PW (right) were transmitted with the same frequency (6 MHz) and MI (0,15). The magnitudes of the RF signals collected by the hydrophone at different positions in the XZ plane are color-coded according to the palette shown on the right. As expected, a considerable difference in the lateral extension of the insonified region can be observed. Similar plots were obtained by varying the TX center frequency within the range of 3–7 MHz.

In the next paragraphs, the harmonics behavior along the beam axis (dashed lines in Fig. 2) is analyzed.

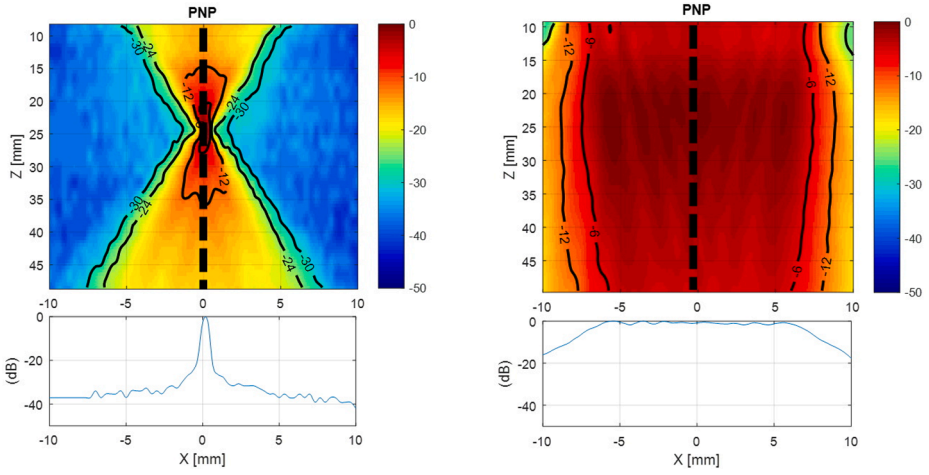

Fig. 2. Normalized XZ beam plots obtained by transmitting 6 MHz pulses with 1 MHz bandwidth focused at 25 mm (top-left) and unfocused (top-right) in quasi-linear conditions (MI = 0.15). The beams axis is highlighted by dashed lines. The bottom panels report the relative amplitudes extracted from the depth of 25 mm.

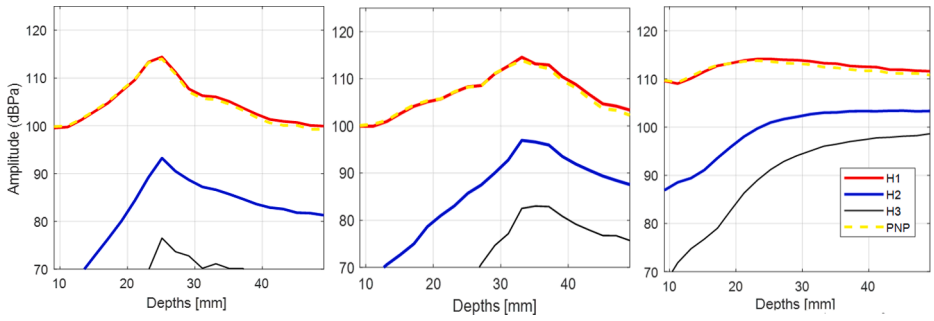

Fig. 3. Total field PNP and 1°, 2° and 3° harmonic peak pressure amplitude measured along the beam axis in a wave focused at 25 mm (left), 35 mm (center) and in PW mode (right), when 6 MHz pulses with 1 MHz bandwidth were transmitted so that 501, 496 and 490 kPa PNP values, respectively, were measured.

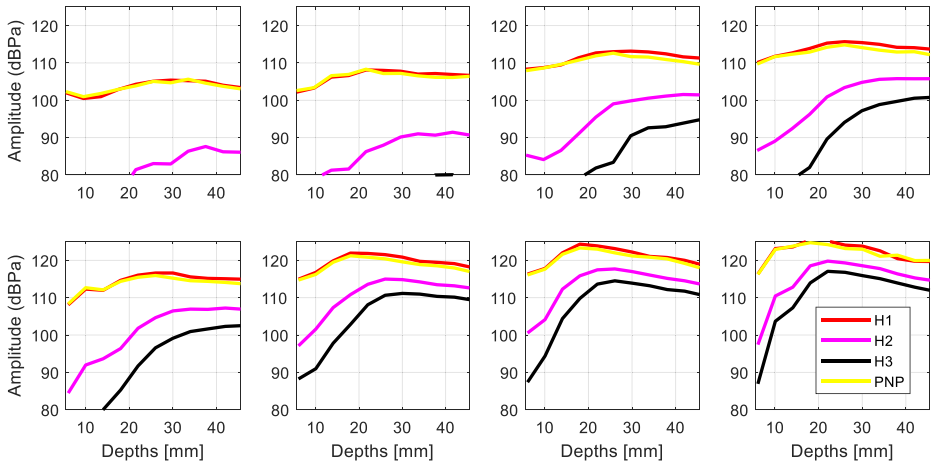

Fig. 4. Total field PNP and 1°, 2° and 3° harmonic peak pressure amplitudes vs. depth in PW when 6 MHz pulses with 1 MHz BW were transmitted with increasing TX power (from left to right and top to bottom MI = 0.07, 0.1, 0.16, 0.20, 0.26, 0.47, 0.60, 0.70 respectively).

2.1.1. *Harmonic amplitude measurements*

The RF ultrasonic signals picked up by the hydrophone were band-pass filtered to highlight the contributions provided by each of the harmonics. Fig. 3 reports the pressure amplitudes measured for the 1st, 2nd, and 3rd harmonics detected along the beam axis when transmitting 25- and 35-mm depth focused waves and plane waves.

At the medium pressure level that was used here (500 kPa), the amplitudes of the first harmonics appear substantially coincident with the PNP amplitude.

When focusing at 25 mm, the amplitudes of the harmonics are very low at shallow depths. The 3rd harmonic, in particular, is very weak, i.e. at least 40 dB lower than the PNP in the focus. The differences between 1st, 2nd, and 3rd harmonic amplitudes are lower in the focal region and remain nearly constant at greater depths.

On the contrary, in PW conditions, strong 2nd and 3rd harmonics are always detected, and their difference from the fundamental component tends to decrease with depth.

By focusing the TX beam at a greater focal depth (35 mm), a behavior intermediate between those visible for FW and PW TX was obtained. This is consistent with the fact that greater focal depths tend to approach the behavior of PWs.

2.1.2. *PW behavior at different MIs*

The influence of transmission power on the PW pressure amplitude detected at different depths is shown in Fig. 4. Here, the harmonics' trends measured at 8 different MIs (from 0,07 to 0,70) are reported.

In most cases, the fundamental component is nearly flat (within 6 dB) at any depth. As expected, by increasing the TX power, the measured pressure amplitudes rapidly increase. Furthermore, the difference between the harmonics, in general, tends to decrease with increasing depth

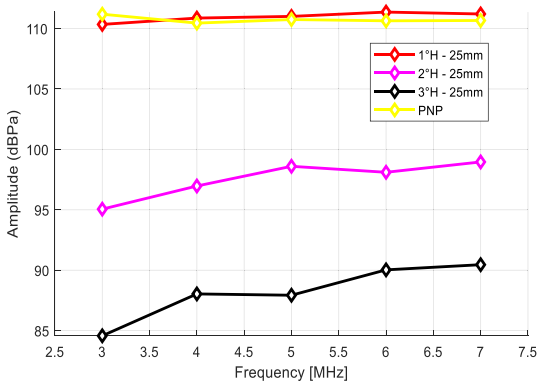

Fig. 5. Total field PNP and 1°, 2° and 3° harmonic peak pressure amplitudes vs. frequency transmitting pulses in the range 3–7 MHz with 1 MHz BW, in PW @ PNP = 360 kPa.

but at higher MIs a minimum value is achieved and then maintained at greater depths. A significant difference between the trends measured at MI < 0.2 and at MI > 0.2 can be observed.

At lowest MIs, the amplitudes of all harmonics monotonically increase until a plateau level (around approximately 30 mm depth) is achieved. At the highest MIs (>0.2), after reaching a peak value around the focal region, the amplitudes of all harmonics tend to markedly decrease. The location of the on-axis peak rarefaction pressure moves towards the transducer with increasing transmission pressure, showing a maximum of 28 mm @ 0.07 MI down to about 18 mm @ 0.70 MI.

Similar results (not shown here for brevity) were obtained at 4 MHz

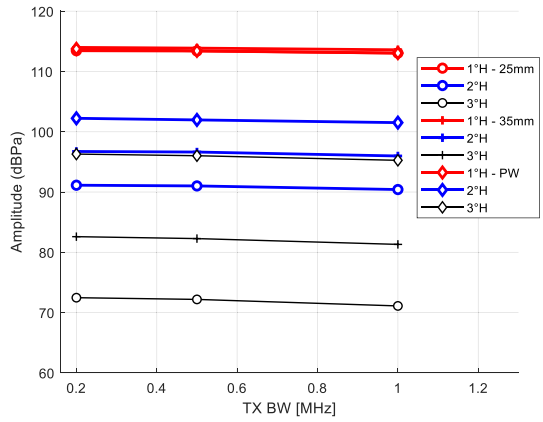

Fig. 6. 1°, 2°, 3° harmonic peak pressure amplitudes measured along the beam axis in the 10–50 mm depth range, in PW and FW @ 25 and 35 mm, when 6 MHz pulses with BW = 0.2, 0.5 & 1 MHz @ MI = 0.16 were transmitted.

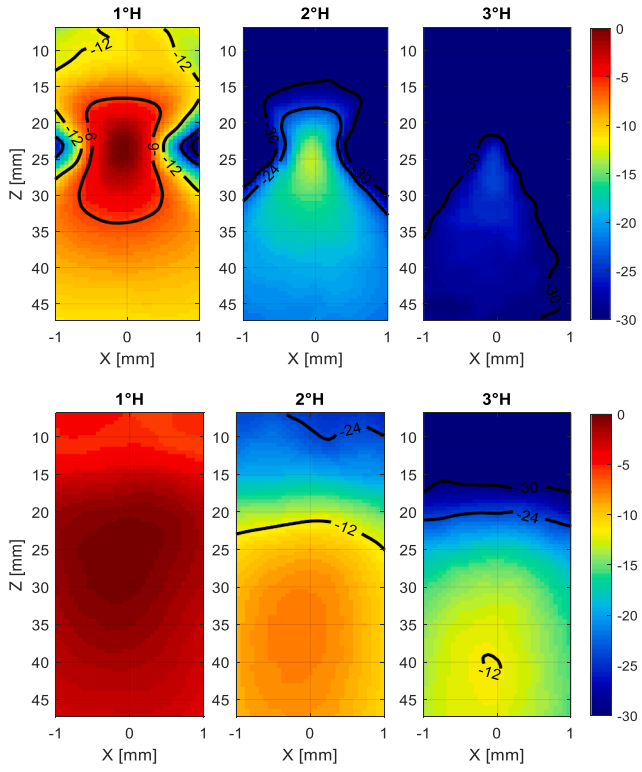

Fig. 7. ZX beamplots over a 2 mm wide region around the beam axis. From left to right: 1st, 2nd and 3rd harmonic amplitudes obtained with 25-mm FW (top) and PW (bottom). (Center frequency = 6 MHz, MI = 0.15).

TX.

2.1.3. PW harmonics behavior at different frequencies

Fig. 5 shows the influence of the TX frequency on the peak pressure amplitudes recorded for each of the first three harmonics.

Special care was taken to equalize the probe behavior, i.e. to obtain the same PNP over the entire range of frequencies.

The graphs show that varying the TX frequency in the range [3–7] MHz, the "distortion" (i.e. the levels of the harmonics) tends to slightly increase with frequency.

2.1.4. Harmonics behavior at different TX bandwidths

Fig. 6 shows the peak pressure amplitudes of the harmonics, measured after transmitting ultrasound bursts with different lengths/bandwidths, focused at 25 mm, 35 mm, and in PW mode.

The non-linear contributions result substantially independent of the TX BW in all investigated conditions.

Table 1
2nd harmonic peak pressure amplitudes for FW (25 mm) and PW TX, @ 2 TX frequencies (4 and 6 MHz) and 3 pressure levels (low = 220 kPa, med = 490 kPa, Hi = 1250 kPa).

F0 – Mode	@ 25 mm [dBPa]			@ 40 mm [dBPa]		
	Low	Med	Hi	Low	Med	Hi
6 - FW	79	91	–	68	82	–
6 - PW	89	100	118	92,5	102	115
4 - FW	73	89	104	61	79	95
4 - PW	83,5	95	114,5	85	96,5	114,5

Table 2
Medium acoustic properties.

Medium	c_0 [m/s]	ρ_0 [Kg/m^3]	B/A	α [dB/MHz^y cm]	y
Water	1482.3	1000	4.96	$2.17 \cdot 10^{-3}$	2
Blood	1584	1060	4	0.14	1.21
Muscle	1580	1041	7.43	0.57	1.01

2.1.5. Behavior around the focal region

The contributions of 1st, 2nd, and 3rd harmonics for both 25-mm FW and PW modes, at MI = 0,14 and 6 MHz TX frequency, over a 2 mm wide region around the beam axes, are reported in Fig. 7.

The bottom panels highlight that previous results obtained for PW TX are not limited to the beam axis. Compared to the FW beam plots obtained at the same (low) MI for a 25 mm focal depth (upper panels), much higher local harmonic contributions are developed. The second harmonic, in particular (mid-lower panel), turns out to be 12 dB below the peak of the fundamental over the entire investigated region.

2.1.6. Experimental results summary

Table 1 summarizes the peak harmonic pressures measured in the different experimental conditions. The table reports the 2nd harmonic amplitudes detected at two depths (25 and 40 mm) by transmitting FWs (with 25 mm focal depth) or PWs at 4 and 6 MHz central frequencies. The second harmonic amplitude is always greater in PW if compared to FW. At a depth of 40 mm, the difference is higher than 17.5 dB in all situations.

3. Simulation study

3.1. Simulation set-up

The K-wave toolbox [14] has been used for the simulation study. Nonlinear ultrasound propagation through two-dimensional homogeneous lossy media was simulated. To model a source like the one used in the experimental study, an array with pitch and kerf equal to 245 and 30 μm, respectively, was simulated. To the same end, a transmitted signal with a bandwidth equal to 1 MHz was modeled.

For both PW and FW, 12 configurations were considered, corresponding to two array sizes (64 and 128 elements), two center frequencies (3 and 4 MHz), and three propagating media (water, blood, and muscle), whose acoustic properties are reported in Table 2 [15]. For each configuration, the pressure fields generated for a range of MI values from 0.05 to 1.2 have been studied. The computational domain depth was set equal to 5 cm and the width was 2.2 and 3.7 cm for the 64- and 128- element array sizes, respectively. For FW TX, the focal depth was set at 25 mm. The computational grid size was $\lambda/7$.

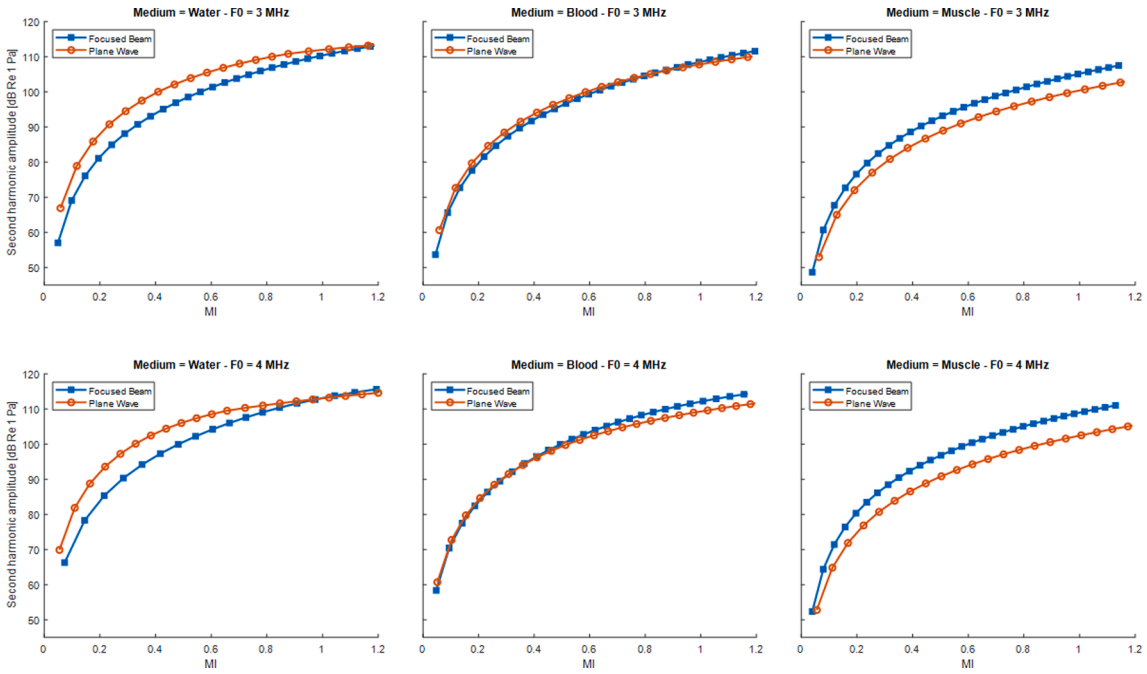

Fig. 8. Second harmonic maximum amplitude expressed in dB relative to 1 Pa vs. MI, as obtained for a 64-element array when transmitting with a center frequency equal to 3 MHz (top row) and 4 MHz (bottom row). Results are shown for PW (red lines) and FW (blue lines) as obtained when ultrasound waves are propagating through water (left column), blood (center column) and muscle (right column).

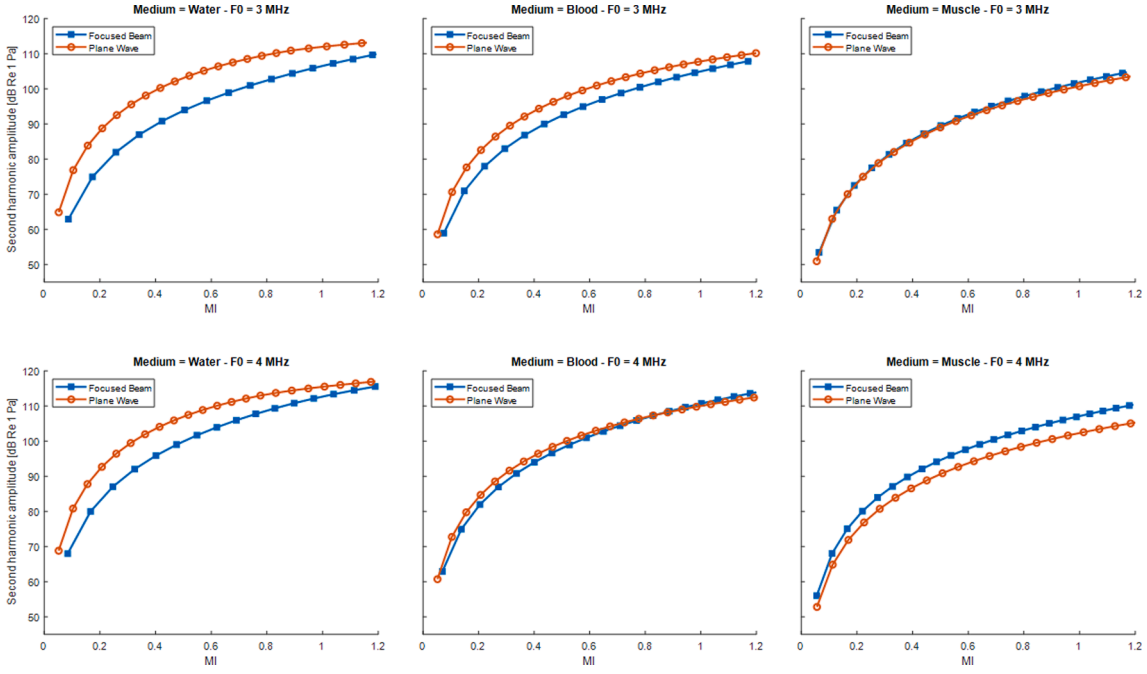

Fig. 9. Second harmonic maximum amplitude expressed in dB relative to 1 Pa vs. MI, as obtained for a 128 elements array when transmitting with a center frequency equal to 3 MHz (top row) and 4 MHz (bottom row). Results are shown for PW (red lines) and FW (blue lines) as obtained when ultrasound waves are propagating through water (left column), blood (center column) and muscle (right column) are shown.

3.2. Simulation Results

Figs. 8 and 9 show the peak second harmonic amplitudes evaluated for the 64- and 128-element array, respectively. Note that the two values reported for each specific MI are, in general, obtained at different depths (the second harmonic peak amplitude obtained over the simulated domain is considered), and therefore are not indicative of the "local" pressure difference. Second harmonic amplitudes achieved with PW (red lines) and FW (blue lines) for ultrasound waves propagating through water (left column), blood (center column), and muscle (right column) are reported. Results obtained when transmitting with a center frequency equal to 3 MHz and 4 MHz are grouped in the top and bottom row, respectively.

Fig. 10 shows the minimum and maximum difference between the second harmonic peak amplitudes obtained with PW and FW TX for the 12 analyzed configurations over the investigated MIs.

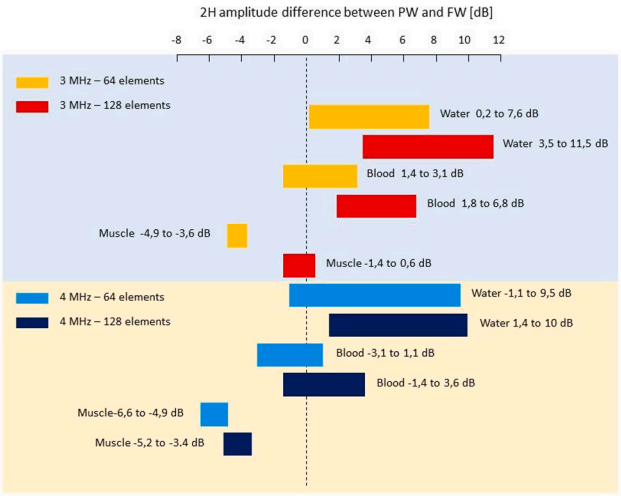

Fig. 10. Second harmonic peak amplitude difference between PW and FW evaluated over the entire MI range (0.05–1.2).

As it can be observed from Figs. 8, 9, and 10, while increasing absorption levels seem to favor FW, increasing the array size favors PW. Interestingly, when a 128 elements array and a center frequency of 3 MHz are used, the second harmonic amplitude can be higher for PW even for ultrasound waves propagating through the muscle.

Fig. 11 shows examples of the pressure profiles along the beam axis when considering a 64 (left column) and 128 (right column) elements aperture. These plots were obtained with a center frequency of 4 MHz and MI equal to 0.5, and are displayed for PW (top) and FW with focus at 25 mm (bottom). Each plot reports the variation of the pressure associated with the first (H1) and second harmonic (H2) at different depths when considering water (blue lines), blood (red lines), and muscle (yellow lines) as propagating media. The effect of the different absorption properties (α and y) on the beam pressure profiles can be observed.

4. Discussion

The experimental results in Fig. 3 and Table 1 show that the amplitudes of the harmonics reached by PW propagation in water are always higher than those achieved by FWs at comparable PNPs, and such difference increases with depth. The amplitudes of the harmonics measured for PWs at MI = 0,1 can be even greater than the amplitudes of the harmonics obtained for FW (25 mm focal depth) at MI = 0,2. The second and third harmonic trends, observed by focusing at a different depth (35 mm), are similar to those obtained by focusing at 25 mm (Fig. 3), with amplitudes at intermediate levels between those measured for FW 25 mm and for PW transmission.

This phenomenon can be explained by the combined effect of 1) the cumulative nature of the waveform steepening process; 2) the larger spatial extension of the region over which high-pressure levels (in the nonlinear regime) are obtained for PW when compared to FW. The PW beam is significantly wider and more homogeneous (see Figs. 2 and 7).

The amplitudes of all PW harmonics monotonically increase with MI until a peak value is achieved (Fig. 4). The depth of the PNP peak was found to decrease at increasing MIs, consistently with the nonlinear focal shift reported in previous work on ultrasound nonlinear propagation [16,17]. It was also observed (Fig. 5) that, like the behavior known for FW mode, the levels of the harmonics tend to slightly increase with the TX frequency in PW mode, while no significant differences were found by varying the TX bandwidth, as shown in Fig. 6.

The experimental findings reported for ultrasound propagation in water are confirmed by numerical studies. At MI < 1, the second harmonic peak amplitude generated with PW is always higher than that generated with FW. Globally, increasing the MI favors FW over PW.

The impact of the array aperture size and frequency-dependent attenuation was evaluated by comparing the second harmonic peak

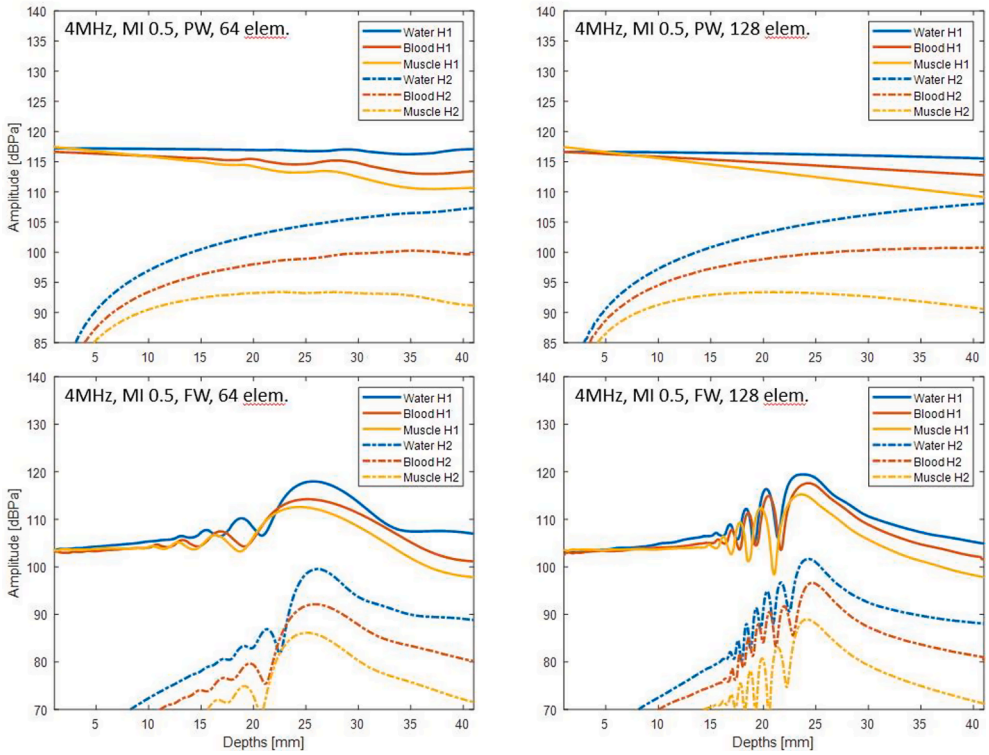

Fig. 11. Harmonics' amplitudes obtained along the beam axis by transmitting pulses with a center frequency of 4 MHz. Plots are shown for PW (top row) and FW with focus at 25 mm (bottom row), as obtained for arrays of 64 (left column) and 128 (right column) elements. The results are reported for first and second harmonics as obtained when ultrasound waves are propagating through water, blood or muscles (yellow lines).

pressures generated by both PW and FW in media (water, blood, and muscle) characterized by different absorption coefficients. Numerical results (Figs. 8-9) show that increasing the array aperture size yields higher harmonic growth in PW compared to FW. This is consistent with the dimensions of the spatial region over which high-pressure amplitudes are generated. Indeed, a larger aperture implies a broader beam for PW and a narrower beam in the case of FW.

As expected, increasing levels of attenuation (due to higher imaging frequency or higher absorbing tissue properties) have different effects on FWs and PWs. The different pressure spatial distribution (i.e., peaked for FWs and monotonic for PWs) affects nonlinear growth and generally favors FW over PW. However, simulations confirm that, even when ultrasound waves are propagating in lossy muscle tissue, the second harmonic peak pressure generated with PWs is comparable or even higher (up to 0.6 dB) than with FWs. This is for instance the case when imaging at 3 MHz with a 128- element array (see Fig. 10). For blood, when imaging at 3 MHz with a 128-element array, the second harmonic peak pressure generated by PW is always higher than that generated by FW, ranging from +1.8 to +6.8 dB. These results may be significant to contrast enhanced ultrasound imaging (CEUS), in which the generation of harmonics due to tissue nonlinearities limits the achievable contrast to tissue ratio. For CEUS, PW is generally considered the method of choice, as it guarantees a relatively spatially homogeneous pressure distribution and a high frame rate, useful to observe contrast dynamics.

5. Conclusion

The main results of this study can be summarized as:

(1) Experiments in water have shown that PW propagation creates harmonics that are significantly high over a wide and deep region, monotonically increase with depth (at MI < 0,2), and (although at a limited extent) with frequency. Compared to the harmonics achieved by FWs at comparable MIs, the amplitudes reached by PWs are always higher, and such difference increases with the distance from the focal point.
(2) Numerical studies (performed for MIs up to 1.2) confirm the experimental findings and indicate that increasing the array size favors higher harmonic growth in PW compared to FW. Simulation results also show how the second harmonic amplitude reached by PWs can still be higher than that achieved by FWs, even in lossy blood and muscle.

These results can have a significant impact when targeting UCA applications, in which the generation of harmonics due to tissue nonlinearities limits the achievable contrast to tissue ratio [10]. The use of PWs could have restrictions in water experiments and for applications in which the field of view is mostly occupied by blood, while it could be the method of choice in lossy tissues [18,19].

Declaration of Competing Interest

The authors declare that they have no known competing financial interests or personal relationships that could have appeared to influence the work reported in this paper.

References

[1] G. Montaldo, M. Tanter, J. Bercoff, N. Benech, M. Fink, Coherent plane-wave compounding for very high frame rate ultrasonography and transient elastography, IEEE Trans. Ultrasonics, Ferroelectrics, Frequency Control 56 (3) (2009) 489–506, https://doi.org/10.1109/TUFFC.2009.1067.
[2] L. Demi, Practical guide to ultrasound beam forming: beam pattern and image reconstruction analysis, Appl. Sci. 8 (9) (2018) 1544, https://doi.org/10.3390/app8091544.
[3] F. Varray, A. Ramalli, C. Cachard, P. Tortoli, O. Basset, Fundamental and second-harmonic ultrasound field computation of inhomogeneous nonlinear medium with a generalized angular spectrum method, IEEE Trans. Ultrasonics, Ferroelectrics, Frequency Control 58 (7) (2011) 1366–1376, https://doi.org/10.1109/TUFFC.2011.1956.
[4] M.A. Averkiou, D.N. Roundhill, J.E. Powers, A new imaging technique based on the nonlinear properties of tissues, in: 1997 IEEE Ultrasonics Symposium Proceedings. An International Symposium (Cat. No.97CH36118), Oct. 1997, vol. 2, pp. 1561–1566 vol.2, doi: 10.1109/ULTSYM.1997.663294.
[5] L. Demi, M.D. Verweij, 2.16 - Nonlinear Acoustics, in: A. Brahme (Ed.), Comprehensive Biomedical Physics, Elsevier, Oxford, 2014, pp. 387–399.
[6] P.L.M.J. van Neer, et al., Comparison of fundamental, second harmonic, and superharmonic imaging: a simulation study, J. Acoust. Soc. Am. 130 (5) (2011) 3148–3157, https://doi.org/10.1121/1.3643815.
[7] L. Demi, K.W.A. van Dongen, M.D. Verweij, A contrast source method for nonlinear acoustic wave fields in media with spatially inhomogeneous attenuation, J. Acoust. Soc. Am. 129 (3) (2011) 1221–1230, https://doi.org/10.1121/1.3543986.
[8] D.T. Blackstock, Propagation of plane sound waves of finite amplitude in nondissipative fluids, J. Acoust. Soc. Am. 34 (1) (1962) 9–30, https://doi.org/10.1121/1.1909033.
[9] I.R.S. Makin, M.A. Averkiou, M.F. Hamilton, Second-harmonic generation in a sound beam reflected and transmitted at a curved interface, J. Acoust. Soc. Am. 108 (4) (2000) 1505–1513, https://doi.org/10.1121/1.1289665.
[10] S. Zhang, X. Li, H. Jeong, S. Cho, H. Hu, Theoretical and experimental investigation of the pulse-echo nonlinearity acoustic sound fields of focused transducers, Appl. Acoust. 117 (2017) 145–149, https://doi.org/10.1016/j.apacoust.2016.10.015.
[11] T.-Y. Lai, M. Bruce, M.A. Averkiou, Modeling of the acoustic field produced by diagnostic ultrasound arrays in plane and diverging wave modes, IEEE Trans. Ultrason. Ferroelectr. Freq. Control 66 (7) (2019) 1158–1169, https://doi.org/10.1109/TUFFC.2019.2908831.
[12] F. Guidi, L. Demi, P. Tortoli, Harmonics amplitude in plane and focused waves - a comparative study at equal mechanical index, in: 2019 IEEE International Ultrasonics Symposium (IUS), Oct. 2019, pp. 2220–2222, doi: 10.1109/ULTSYM.2019.8926003.
[13] P. Tortoli, L. Bassi, E. Boni, A. Dallai, F. Guidi, S. Ricci, ULA-OP: an advanced open platform for ultrasound research, IEEE Trans. Ultrason. Ferroelectr. Freq. Control 56 (2009) 2207–2216, https://doi.org/10.1109/TUFFC.2009.1303.
[14] B.E. Treeby, J. Jaros, A.P. Rendell, B.T. Cox, Modeling nonlinear ultrasound propagation in heterogeneous media with power law absorption using a k-space pseudospectral method, J. Acoust. Soc. Am. 131 (6) (2012) 4324–4336, https://doi.org/10.1121/1.4712021.
[15] T.L. Szabo, Diagnostic Ultrasound Imaging: Inside Out, Elsevier, 2004.
[16] F. Guidi, O. Supponen, A. Upadhyay, H.J. Vos, M.A. Borden, P. Tortoli, Microbubble radiation force-induced translation in plane-wave versus focused transmission modes, IEEE Trans. Ultrason., Ferroelectr., Frequency Control, pp. 1–1, 2019, doi: 10.1109/TUFFC.2019.2937158.
[17] A.F.H. Lum, M.A. Borden, P.A. Dayton, D.E. Kruse, S.I. Simon, K.W. Ferrara, Ultrasound radiation force enables targeted deposition of model drug carriers loaded on microbubbles, J. Control. Release 111 (1–2) (2006) 128–134, https://doi.org/10.1016/j.jconrel.2005.11.006.
[18] F.A. Duck, H.C. Starritt, The locations of peak pressures and peak intensities in finite amplitude beams from a pulsed focused transducer, Ultrasound Med. Biol. 12 (5) (1986) 403–409, https://doi.org/10.1016/0301-5629(86)90198-5.
[19] M. Versluis, E. Stride, G. Lajoinie, B. Dollet, T. Segers, Ultrasound contrast agent modeling: A review, Ultrasound Med. Biol. (2020), https://doi.org/10.1016/j.ultrasmedbio.2020.04.014.